Optimal design and performance analysis of a hybrid system combing a floating wind platform and wave energy converters

Jianjian Hu [a], Binzhen Zhou [a,b,c*], Christopher Vogel [b], Pin Liu [a], Richard Willden [b], Ke Sun [a], Jun Zang [d], Jing Geng [a], Peng Jin[a], Lin Cui [e], Bo Jiang [e] , Maurizio Collu [f]

[a]*College of Shipbuilding Engineering, Harbin Engineering University, Harbin 150001, China*
[b]*Department of Engineering Science, University of Oxford, OX1 3PJ, UK*
[c] *Shandong Provincial Key Laboratory of Ocean Engineering, Ocean University of China, Qingdao 266100, China*
[d]*Department of Architecture and Civil Engineering, University of Bath, Bath, BA2 7AY, UK*
[e] *National Ocean Technology Center, Tianjin 300112, China*
[f] *Naval Architecture, Marine and Ocean Engineering, University of Strathclyde, Glasgow, G4 0LZ, UK*

Abstract

Combined floating offshore wind platform and Wave Energy Converters (WECs) systems have the potential to provide a cost-effective solution to offshore power supply and platform protection. The objective of this paper is to optimize the size and layout of WECs within the hybrid system under a given sea state with a numerical study. The numerical model was developed based on potential flow theory with viscous correction in frequency domain to investigate the hydrodynamic performance of a hybrid system consisting of a floating platform and multiple heaving WECs. A non-dimensional method was presented to determine a series of variables, including radius, draft, and layout of the cylindrical WEC at a typical wave frequency as the initial design. WECs with larger diameter to draft ratio were found to experience relatively smaller viscous effects, and achieve more wave power, larger effective frequency range and similar wave power per unit weight compared with those with the smaller diameter to draft ratio in the same sea state. The addition of WECs reduced the maximum horizontal force and pitch moment on the platform, whereas the maximum vertical force increased due to the increasing power take-off force, especially at low frequencies. The results presented in this paper provide guidance for the optimized design of WECs and indicate the potential for synergies between wave and wind energy utilization on floating platforms.

Keywords: Floating platform; Wave energy converter; Hybrid system; Wave power;

* Corresponding author
E-mail address: zhoubinzhen@hrbeu.edu.cn (B.Z. Zhou)

Hydrodynamic performance; Viscous.

1. Introduction

Offshore wind energy has been rapidly developing in recent years due to the fact that wind is stronger and steadier at the sea than on the land, and the availability of space for wind farm installation [1]. Wave energy is one of the most promising renewable energy resources because of its high energy density, predictability, and wide-spread availability [2], which similarly has a much higher power density in deep water regions (about larger than 200 m) [3]. Deep water offshore deployment of wind and wave energy is only at an early stage of development due to the challenges of high design, installation, operation, and maintenance costs. The combined exploitation of offshore wind power and ocean wave energy has been proposed as one way of helping to reduce cost [4].

There are multiple benefits of the hybrid system of a floating offshore wind energy and Wave Energy Converters (WECs). Firstly, integrating WECs with an offshore wind platform (wind-wave hybrid system) can improve the energy output per square meter due to the shared ocean space [5]. Secondly, it can reduce the overall project cost by sharing the mooring system, power infrastructure, and other components of the wind farm. Thirdly, wave energy production may compensate for the intermittency of offshore wind, i.e., the hybrid system can reduce the hours of zero production compared with a stand-alone wind turbine, as ocean waves tend to persist even after the wind dies away [6]. In addition, an efficient layout of WECs can modify the local wave climate, providing a sheltered environment for operation and maintenance, which will effectively protect the offshore wind platform from heavy wave loads during storm conditions [7].

Due to the above mentioned benefits provided by the wind-wave hybrid system, the combined exploitation of wave and offshore wind energy has become a hot research topic in recent years [4]. Depending on the support structure design, the hybrid system can be classified into bottom-fixed and floating types, which are appropriate for shallow (about smaller than 20m) or moderate (between 20 m and 200 m) and deep water (about larger than 200 m) respectively [3]. Recently, a number of bottom-fixed wind-wave hybrid systems have been proposed: Wave Star [8], Wave Treader [9] and WEGA [10]. The floating offshore wind turbine (FOWT)-wave hybrid system is a new concept that has come under consideration with the advent of floating offshore wind prototypes in recent years. The EU FP7 MARINA platform project [11] proposed three conceptual designs of FOWT-WECs combinations and studied them numerically and experimentally under operational and extreme conditions. The three concepts were the spar torus combination (STC) [12], the semi-submersible flap

combination (SFC) [13], and an array of oscillating water columns (OWC) [14] in a V-shaped concrete large floating platform with one 5 MW NREL wind turbine (WT) [15]. Three different WEC types have been integrated with WindFloat, including an OWC type WEC [16], a spherical wave energy device [17], and an oscillating wave surge converter [18]. Pelagic Power AS proposed the floating hybrid W2 power, consisting of a semi- submersible platform, two wind turbines and an array of heaving point absorb floats [19].

Moreover, based on the linear potential flow theory with viscous correction in frequency domain, Lee et al. [20] put forward a mathematical model of a floating platform and multiple WECs to study the dynamic response of a 10MW-class wind-wave hybrid power generation system which has four wind turbines at each corner of the semi-submersible and 24 WECs along the side, designed by Kim et al. [21]. Taghipour & Moan [22] developed a mode expansion method to investigate the interaction of 21 heaving point absorbers in a floating platform, known as the FO^3 device. The method was found to be computationally efficient and easier to interface with structural code compared to the available standard procedures by means of multi-body analysis approach. De Backer et al. [23] studied numerically the performance of two array layouts of 12 heaving buoys in a staggered grid and 21 heaving buoys in an aligned grid in frequency domain. Three strategies to determine the control parameters for multiple WECs were compared: the optimal control values for a single buoy, diagonal optimization (DO) and individual optimization (IO). The latter two strategies were both better than the first one. Compared to DO, IO increased the energy absorption at Westhinder with about 16-18% for the two layouts, respectively. Sarmiento et al. [24] experimentally studied the performance of a multi-use triangular semi-submersible platform equipped with a 5MW wind turbine supported in the central column and three OWCs placed around the external columns under the incidence of regular wave tests (with and without wind), operational sea states and survival sea states (combining waves, currents and wind). The results showed that the wind turbine introduced higher motions of the platform and mooring system loads, while the normal operation of the OWCs had limited influence in the platform's dynamics. Michele et al. [25] developed a mathematical model to analyze the hydrodynamics of a novel OWC in a hybrid wind-wave energy system in regular and random waves, and validated it with the experiment by Perez-Collazo et al. [26]. The numerical study showed that the skirt of the external cylinder had strong effects on the global behavior, while the internal cylinder affected the values of the sloshing eigenfrequencies. These studies have shown that adding WECs could increase the total power production compared to the stand-alone FOWT, and the effects of WECs on platform motion have also been investigated.

Previous studies have primarily focused on the impact of a specified size and layout of WECs on the motion of a floating platform. For example, Lee et al. [20] found that platform response was only minimally affected by power take-off (PTO) damping, although only one small level of PTO damping was considered. Most numerical simulations have been carried out based on potential flow theory, which allows an initial understanding of the hydrodynamic fundamentals of the hybrid system to be developed, however it highly overestimates the motion and power response of a point absorber WEC as viscous effects are neglected [27]. Especially around the resonance frequency of WECs, the response simulated by non-viscous linear potential flow theory can be 10 times or larger than that of equivalent experiments [28]. An alternative approach is to use Computational Fluid Dynamics (CFD) methods [29], which are able to deal with strongly nonlinear phenomena, such as vortex shedding and turbulence. However, the computational cost of detailed CFD simulations is high due the large computational meshes required, and thus potential flow theory with a viscous correction provides a tractable way to conduct an initial optimization, supported by detailed CFD of selected cases. The numerical and experiment studies of Tom [28] and Son et al. [30] for a heaving point absorber WEC illustrated that the exciting forces can be well predicted by linear potential flow theory, while the radiation forces (especially the damping term) were significantly affected by viscous effects, and must therefore be accounted for. The viscous hydrodynamic coefficients can be obtained from the experiment [20][28][30][31] or the CFD results [32] of the free decay test.

It is not possible to generalize the effect of adding WECs to a floating platform from existing studies. The motivation and novelty of this work is twofold; firstly to develop an efficient and accurate method to optimize the size and layout of WECs on a platform for a given sea state, and secondly to obtain a more comprehensive understanding of the influence of adding WECs to a floating platform through a series of studies. This will help lead to cost-sharing WEC-platform solutions that help reduce the overall cost of wave energy.

The paper is structured as follows. Section 2 presents the details of the floating wind platform, WECs, and the given wave environment. Section 3 introduces the establishment of a multi-body mathematical model based on potential flow theory with viscous correction in frequency domain. The optimal design and hydrodynamic performance of the hybrid system combing a floating wind platform and multiple heaving WECs are carried out, and the results are presented in Section 4. The accuracy of the numerical model is verified through the comparison with the published numerical results. A non-dimensional method is presented to determine a series of parameters, including radius, draft, and layout of the cylindrical WEC at a typical wave frequency as the initial design. The effects of the diameter to draft ratio of

WECs on wave power, wave power per unit weight, and the forces on the platform are investigated. Finally, the conclusions are presented in Section 5.

2. Configuration of platform and WECs

2.1 Floating wind platform

The WindFloat platform [33] with a 5 MW wind turbine, a floating semi-submersible triangular platform patented in 2003 by the offshore engineering consulting company MI & T (Marine Innovation & Technology) is chosen for the case study in this paper. Fig. 1 shows the configuration of the structure, consisting of column-stabilized offshore platform with water-entrapment plates, one wind turbine, and an asymmetric mooring system. A wind turbine mast is positioned directly above one of the stabilizing columns. Its main dimensions are listed in Table 1.

Fig. 1 The WindFloat platform [33].

Table 1 Main dimensions of WindFloat [33]

Item	Symbol	Value	Unit
Column radius	R	5.35	m
Column center to center	L	56.4	m
Total platform height		33.6	m
Operating draft	D	22.9	m
Length of heave plate edge	B	13.7	m
Height of hexagonal damping plate	d_2	0.1	m
Pontoon diameter		1.8	m
Bracing diameter		1.2	m
Displacement		7.105×10^6	kg

2.2 Wave energy converters

WECs are installed on the sides of the platform between the trusses. The typical cylindrical float with a flat bottom is chosen as the WEC. Fig. 2 shows a sketch of a hybrid system

combing a WindFloat platform and multiple heaving WECs with the PTO system connected between each WEC and the platform. Each WEC is designed to move vertically along the fixed guide cylinder and generates electricity through the relative heave motion against the platform. All WECs in the system are of similar size and equally spaced along each truss. The radius and draft of each WEC are defined as r and d, respectively, and the distance between adjacent WECs is L_1. The distance between the column of the platform and the adjacent WEC is L_2. Different ratios of diameter to draft and different numbers of WECs are considered in this study.

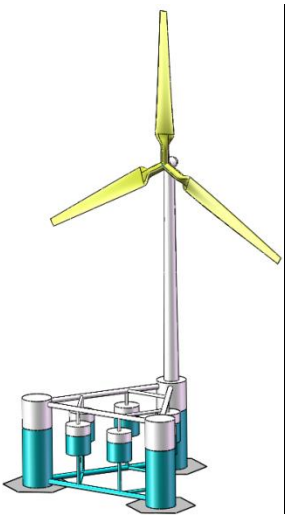

Fig. 2 Hybrid system of a floating wind platform and multiple heaving WECs

2.3 Wave environments

The wave environments of the sea area around Shandong province in China were obtained in a field study and are used as a reference for system evaluation. The joint probability distribution S_i of the wave height H_i and the wave period T_i is given in Table 2. It can be seen that wave periods are mainly in the range of 4 s-6 s, which is therefore targeted for good WEC performance. The average wave period is T=4.94 s (ω=1.27 rad/s), and the average wave height is H=0.84 m, which will be used for the initial design of WECs to obtain the maximum wave power.

Table 2 Joint distribution S_i of wave height H_i and wave period T_i in the sea area around Shandong province, China (Unit: %)

H_i (m)\ T_i(s)	3	4	5	6	7	8	9	10	11	12	13	14	sum
0.25	0.033	0.164	0	0	0	0	0	0	0	0	0	0	
0.5	3.435	12.267	4.907	0.425	0	0	0	0	0.032	0	0	0	0.196
1	1.930	14.884	21.851	11.220	2.355	0.425	0.327	0.098	0.032	0	0	0	21.066
1.5	0.033	0.556	3.500	5.528	3.729	0.883	0.392	0.262	0.196	0	0	0	53.124
2	0	0.033	0.425	2.028	2.289	0.883	0.164	0.458	0.098	0	0.065	0	15.080
2.5	0	0	0	0.360	0.883	0.916	0.229	0	0.098	0.065	0	0	6.444

3	0	0	0	0	0.392	0.360	0.196	0.033	0	0	0	0.0654	2.552
3.5	0	0	0	0	0	0.131	0.196	0	0	0	0	0	1.047
4	0	0	0	0	0	0.033	0.065	0.033	0	0.033	0	0	0.327
4.5	0	0	0	0	0	0	0	0	0	0	0	0	0.0
5	0	0	0	0	0	0	0	0	0	0	0	0	0
5.5	0	0	0	0	0	0	0	0	0	0	0	0	0
6	0	0	0	0	0	0	0	0	0	0	0	0	0
6.5	0	0	0	0	0	0	0	0	0	0	0	0	0
7	0	0	0	0	0	0	0	0	0	0	0	0	0
sum	5.430	27.903	30.684	19.562	9.650	3.631	1.570	0.883	0.458	0.098	0.065	0.065	100.0

3. Mathematical Model

3.1 Motion equation of WECs

The linear method is typically used for the initial design of floating offshore structures, because it can quickly and simply estimate the performance of the hybrid system [20] [22] [23] [25]. Zhou et al. [34] and Zhou & Wu [35] have conducted numerical studies on the fully nonlinear wave interactions with floating cylinder and Tension leg platform. The results showed that the nonlinear theory was necessary only when the contribution from the higher harmonic term was great, such as springing and ringing. The WECs work as the first harmonic wave frequency is close to the resonance frequency, so the contribution from the first harmonic wave is much more important than that from other harmonic terms. Therefore, the linear theory is accurate enough for the initial design of WECs, but not suitable for the cases under extreme sea conditions. The further detailed design requires more accurate and sophisticated analysis, including nonlinear terms.

To constrain the degrees of freedom for the initial design, the platform is assumed to be fixed because its motion is relatively small compared with that of WECs. Since each WEC moves in heave mode only, the equation of motion for the *i*-th WEC can be written as

$$\left[-\omega^2(m_i+\mu_{ii})-\mathrm{i}\omega\left(\lambda_{ii}+b_{\mathrm{pto},i}+\lambda_{\mathrm{vis},i}\right)+(k_{\mathrm{pto},i}+C_i)\right]z_i+\sum_{j=1,\ j\neq i}^{N}(-\omega^2\mu_{ij}-i\omega\lambda_{ij})z_j=F_{\mathrm{ex},i} \tag{1}$$

which can also be expressed in the following matrix

$$\left\{-\omega^2\left(\begin{bmatrix} m_1 & & \\ & \ddots & \\ & & m_N \end{bmatrix}+\begin{bmatrix} \mu_{1,1} & \cdots & \mu_{1,N} \\ \vdots & \ddots & \vdots \\ \mu_{N,1} & \cdots & \mu_{N,N} \end{bmatrix}\right)\right.$$
$$\left.-i\omega\left(\begin{bmatrix} \lambda_{1,1} & \cdots & \lambda_{1,N} \\ \vdots & \ddots & \vdots \\ \lambda_{N,1} & \cdots & \lambda_{N,N} \end{bmatrix}+\begin{bmatrix} b_{\mathrm{pto},1} & & \\ & \ddots & \\ & & b_{\mathrm{pto},N} \end{bmatrix}+\begin{bmatrix} \lambda_{\mathrm{vis},1} & & \\ & \ddots & \\ & & \lambda_{\mathrm{vis},N} \end{bmatrix}\right)+\begin{bmatrix} k_{\mathrm{pto},i}+C_1 & & \\ & \ddots & \\ & & k_{\mathrm{pto},N}+C_N \end{bmatrix}\right\}\begin{bmatrix} z_1 \\ \vdots \\ z_n \end{bmatrix}=\begin{bmatrix} F_{\mathrm{ex},1} \\ \vdots \\ F_{\mathrm{ex},N} \end{bmatrix} \tag{2}$$

where ω is the wave frequency; i is the imaginary unit; m_i is the mass of the *i*th WEC; C_i, $k_{\mathrm{pto},i}$, $b_{\mathrm{pto},i}$, $F_{\mathrm{ex},i}$ and z_i are the restoring force, the elastic stiffness and mechanical damping due to the PTO system, the wave exciting force, and the heave motion of the *i*th WEC, respectively. μ_{ij} and λ_{ij} are the added mass and radiation damping of the *i*th WEC in the heave mode due to

the heave motion of the *j*th WEC based on the potential flow theory, respectively. $\lambda_{\mathrm{vis},i}$ is the corrected viscous damping of the *i*th WEC in the heave mode at the natural frequency, and *N* is the total number of WECs in the hybrid system. μ_{ij}, λ_{ij} and $F_{\mathrm{ex},i}$ are calculated by a higher-order boundary element method (HOBEM) code package WAFDUT. The program WAFDUT is used to solve the diffraction and radiation problems of multi-bodies with arbitrary shapes based on the linear potential flow theory in frequency domain [36][37].

3.2 Viscous correction of WECs

The viscous effect is very important for WECs because the motion response will be overestimated near the natural frequency if potential flow theory is used. The linear damping corrections $\lambda_{\mathrm{vis},i}$ are added into Eq. (1) to consider the viscous effect, which can be obtained through free decay experiments.

The non-dimensional damping κ is given by [20]

$$\kappa = \frac{1}{2\pi} \ln \frac{z_{a_k} - z_{a_{k+1}}}{z_{a_{k+2}} - z_{a_{k+3}}} \tag{3}$$

where z_{a_k} and $z_{a_{k+2}}$ are the two successive positive maximum displacements; $z_{a_{k+1}}$ and $z_{a_{k+3}}$ are the two successive negative maximum displacements. The total damping coefficient can be obtained as

$$\lambda_{\mathrm{vist}} = \frac{2\kappa C}{\omega_n} \tag{4}$$

where *C* and ω_{n} are the hydrostatic coefficient and the natural frequency, respectively. The total damping including the potential and viscous parts can be estimated from the decaying oscillation by determining the ratio between any pair of successive (double) amplitudes. In the present paper, the first three pairs are choosen to obtain the average value.

The viscous damping correction coefficient for the *i*th WEC is

$$\lambda_{\mathrm{vis},i} = \lambda_{\mathrm{vist},i} - \lambda_{ii} \tag{5}$$

The non-dimensional linearized viscous damping correction is defined as

$$f_{\lambda,\mathrm{vist}} = \lambda_{\mathrm{vist},i} / \lambda_{ii} \tag{6}$$

where $f_{\lambda,\mathrm{vist}}$ is the corrected ratio of the total viscous damping to the potential damping.

3.3 Optimal PTO damping and wave power of WECs

The resonance frequency is defined as the natural frequency of the body when the inertial force and the restoring force are in equilibrium, so the natural frequency of the *i*th WEC in the heave mode can be written as [38]

$$\omega_{n,i} = \sqrt{\frac{k_{\text{pto},i} + C_i}{m_i + \mu_{ii}(\omega_{n,i})}} \tag{7}$$

For a single body with only one mode of motion, the optimal damping coefficient of the ith body $b_{\text{opt},i}$ under wave frequency ω can be written as [38]

$$b_{\text{opt},i} = \sqrt{\frac{((m_i + \mu_{ii})\omega^2 - (k_{\text{pto},i} + C_i)^2}{\omega^2} + (\lambda_{ii} + \lambda_{\text{vis},i})^2} \tag{8}$$

The wave power $P_i(\omega)$ at wave frequency ω produced by the ith WEC is derived by

$$P_i(\omega) = \frac{1}{2}\omega^2 b_{\text{pto}} |z_i|^2 \tag{9}$$

Then the total wave power $P_{\text{total}}(\omega)$ of the WEC array is

$$P_{\text{total}}(\omega) = \sum_{i=1}^{N} P_i(\omega) \tag{10}$$

To choose the optimal size and layout of WECs, the wave power per unit weight P_{av} is introduced as the ratio

$$P_{\text{av}}(\omega) = \frac{P_{\text{total}}(\omega)}{\rho V_{\text{total}}} \tag{11}$$

where ρ=1023 kg/m^3 represents the fluid density, ρV_{total} is the total displacement of the WECs, which is equal to the total weight of WECs. The larger P_{av}, the higher the economic efficiency of the device.

The total wave power $P_{\text{total(year)}}$ and the wave power per unit weight $P_{\text{av(year)}}$ in one year are introduced to evaluate the energy capture performance of WECs in the target sea area, as shown in Table 2,

$$P_{\text{total(year)}} = \sum_{j=1}^{M} (\frac{H_j}{2})^2 \times P_{\text{total}}(T_j) \times S_j \tag{12}$$

$$P_{\text{av(year)}} = \frac{P_{\text{total(year)}}}{\rho V_{\text{total}}} \tag{13}$$

where T_j, H_j, and S_j are the wave period, the wave height, and the probability of the jth wave component in Table 2; $P_{\text{total}}(T_j)$ is the total power per unit wave height of the WEC array at wave period T_j; and M is the total number of waves components in Table 2.

To quantify the effect of wave interactions on wave power in a WEC array, the mean interaction factor q_{mean}, defined as the ratio of the total wave power of the array to N times wave power from a single isolated WEC, is introduced [39]

$$q_{\text{mean}}(\omega)=\frac{P_{\text{total}}(\omega)}{N\times P_{\text{isolated}}(\omega)} \tag{14}$$

where $P_{\text{isolate}}(\omega)$ is the maximum wave power of an isolated WEC at the wave frequency ω, obtained using the optimal PTO damping. If $q_{\text{mean}}<1$, the average WEC power in the array is less than the power of an isolated WEC, as the wave interactions have a destructive effect on the power absorption of the wave farm. Conversely, if $q_{\text{mean}}>1$, the farm effect is constructive.

3.4 Non-dimensionalization

The draft of the WEC d is taken as the reference length scale for non-dimensionalization. $k_{\text{pto},i}$ is neglected to reduce the number of unknowns. The non-dimensional radius, mass and restoring force can be written as

$$\bar{r}=\frac{r}{d};\qquad \bar{m}_i=\frac{m_i}{\rho g\pi r^2 d}=1;\qquad \bar{C}_i=\frac{C_i}{\rho g\pi r^2}=1 \tag{15}$$

The non-dimensional added mass, radiation damping and wave exciting force can be written as

$$\bar{\mu}_{ij}=\frac{\mu_{ij}}{\rho g\pi r^2 d};\qquad \bar{\lambda}_{ij}=\frac{\lambda_{ij}}{\rho\pi r^2\sqrt{gd}};\qquad \bar{F}_{\text{ex},i}=\frac{F_{\text{ex},i}}{\rho g\pi r^2 d} \tag{16}$$

The non-dimensional natural frequency can be written as

$$\bar{\omega}=\frac{\omega}{\sqrt{g/d}} \tag{17}$$

where g=9.807 m/s^2 denotes acceleration due to gravity.

The non-dimensional natural frequency for a given $2r/d$ can be calculated by

$$\bar{\omega}_{n,i}(2r/d)=\sqrt{\frac{1}{1+\bar{\mu}_{ii}\left(\bar{\omega}_{n,i}(2r/d)\right)}} \tag{18}$$

The maximum wave power of the WEC array is obtained when the wave frequency ω_{n} is equal to its natural frequency, so the WEC size can be determined according to the typical or average wave frequency ω_{p} of the wave environment. Following Eqs. (7), (17) and (18), the draft of WEC can be determined for a given $2r/d$

$$d=g\left(\frac{\bar{\omega}_n(2r/d)}{\omega_{\text{p}}}\right)^2 \tag{19}$$

Therefore, for a given ω_{p}, a series of draft d and radius r of the cylindrical float can be

obtained and further evaluated according to Eq. (19). The total wave power P_{total} and the wave power per unit weight P_{av} are used to evaluate the optimal WEC array.

4. Numerical results and discussions

4.1 Verification

To validate the present numerical model, a 5×1 hemispherical WEC array by Bellew [40] is simulated. Each hemispherical WEC with the same radius r only oscillates in heave mode. The WEC-WEC spacing of 4r and a water depth of 7r were considered. The mass of each WEC was twice the displacement of the WEC. Fig. 3 shows the mesh of the five hemispherical WECs, where 150 elements were used for each hemisphere following the mesh convergence study. Fig. 4 shows the comparison of the mean interaction factor q_{mean} for the WEC array under the optimal PTO damping calculated by Eq. (8), where the added mass μ_{ii} and radiation damping λ_{ii} were calculated by a single hemispherical WEC, similar to Bellew [40]. It can be seen that the present results are in good agreement with the published numerical results.

Fig. 3 Mesh of the five hemispherical WEC devices.

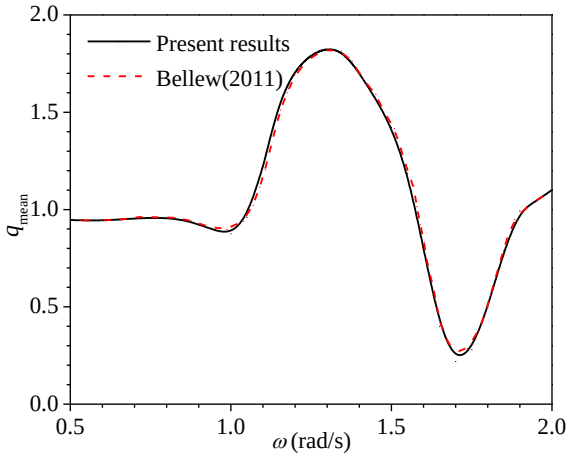

Fig. 4 Comparison of the mean interaction factor between the present results and the published numerical results in [40].

4.2 Geometric configurations and layout selection of WECs

Fig. 5 (a-c) shows the non-dimensional added mass, radiation damping, and exciting forces of a single cylindrical WEC calculated by the code package WAFDUT. The non-dimensional natural frequency can be calculated based on Eq. (7), as shown in Fig. 5 (d), which provides an important guide for the selection of the size and layout of WECs. As the diameter to draft

ratio $2r/d$ increases, the non-dimensional added mass and radiation damping increase nearly linearly, while the non-dimensional exciting force and the natural frequency of the WEC decrease nearly linearly. Reducing the ratio of $2r/d$ is therefore a good way to lower the non-dimensional natural frequency of the float.

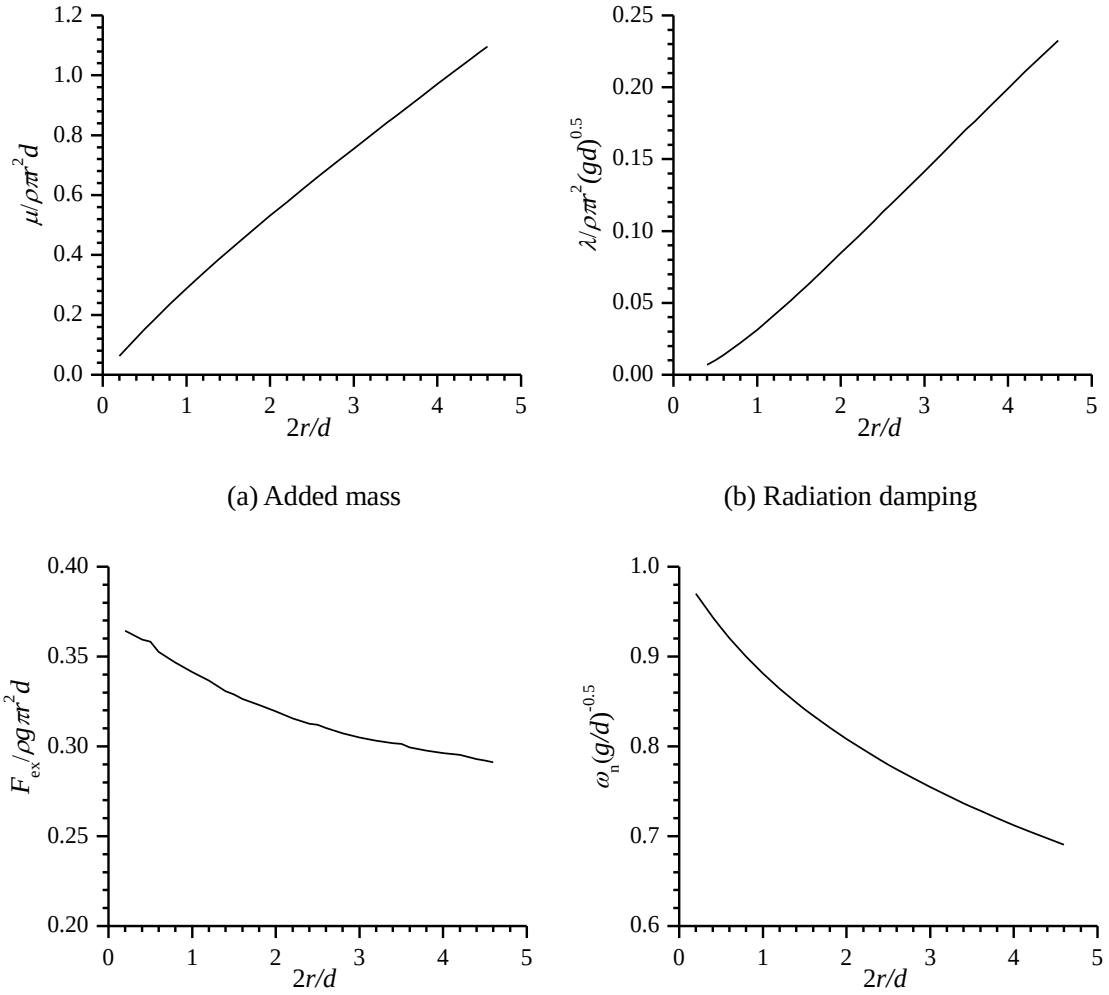

(a) Added mass (b) Radiation damping

(c) Exciting force (d) Natural frequency

Fig. 5 Variation of non-dimensional added mass, radiation damping, exciting force and natural frequency of cylindrical float versus $2r/d$.

Taking the average wave period of a sea area T_p=4.94 s in China as an example, the size of the cylindrical WEC will be determined to capture the maximum wave power at the average wave period. According to the working principle of a point absorber WEC, $\omega_p=2\pi/T_p$ is the natural frequency of the cylindrical WEC in the heave mode. The draft of the cylindrical WEC can be determined by Eq. (19) for different $2r/d$, as shown in Fig. 6 (a). Next, the layout of WECs on the platform is determined according to the platform size and the distance between column centers. In addition, to reduce the mutual interference between adjacent WECs and columns, the distance L_1 is set as $4r$ and L_2 must be larger than $(R+2r)$. Therefore,

the maximum number N_L of WECs on one side of the truss is taken as an integer (L-2R)/4r, as shown in Fig. 6 (b), and the corresponding L_1 and L_2 are shown in Fig. 6 (c).

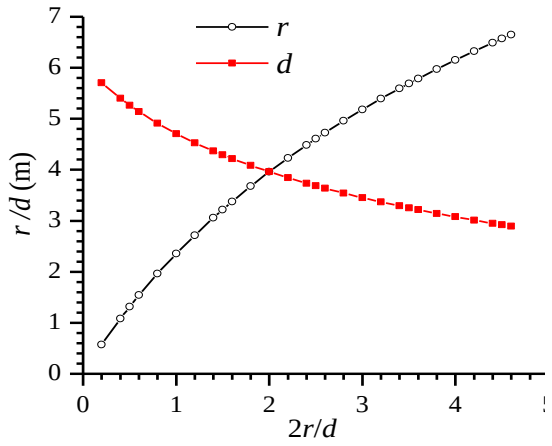

(a) Radius and draught of float

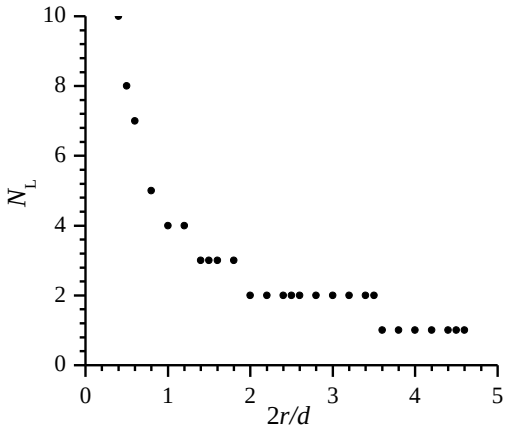

(b) Number of WECs in one truss

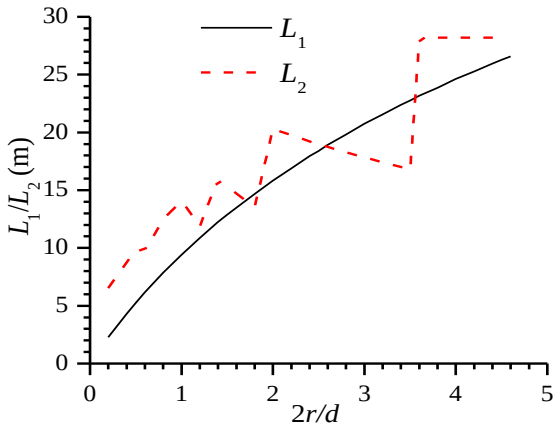

(c) Distance L_1 and L_2

Fig. 6 The size and layout of initial selected WECs for T_p=4.94 s.

4.3 Variation of hydrodynamic coefficients of WECs

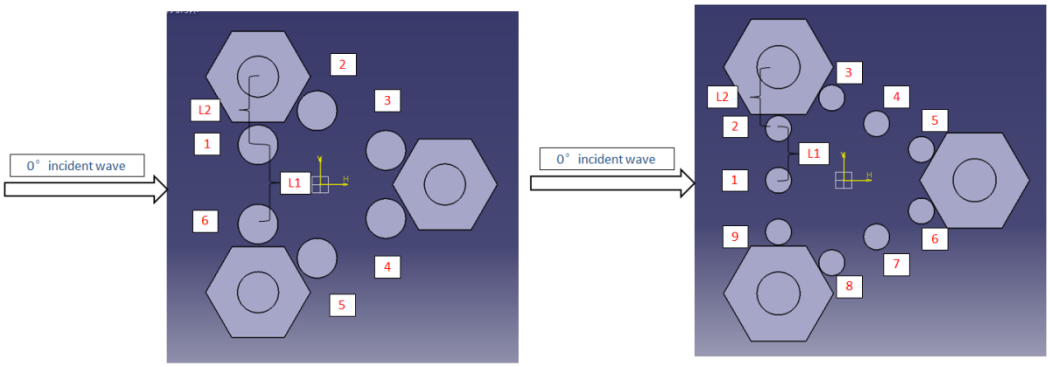

(a) 6 WECs (b) 9 WECs

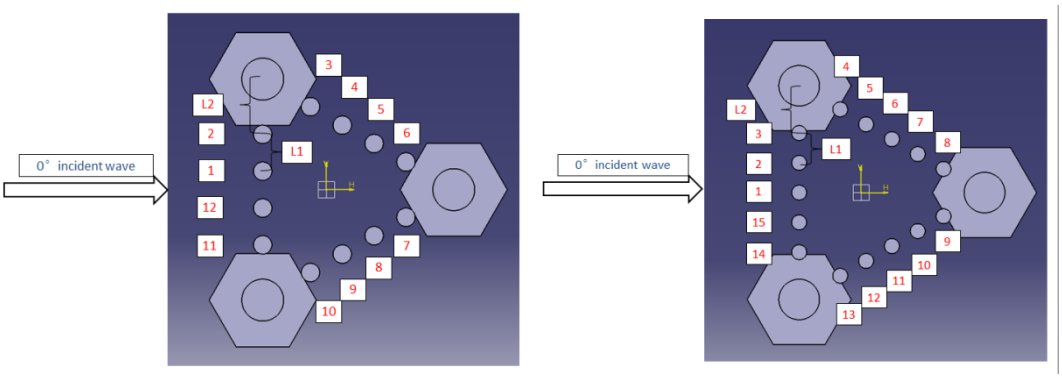

(c) 12 WECs (d) 15 WECs

Fig. 7 Plan view of four different layouts of WECs.

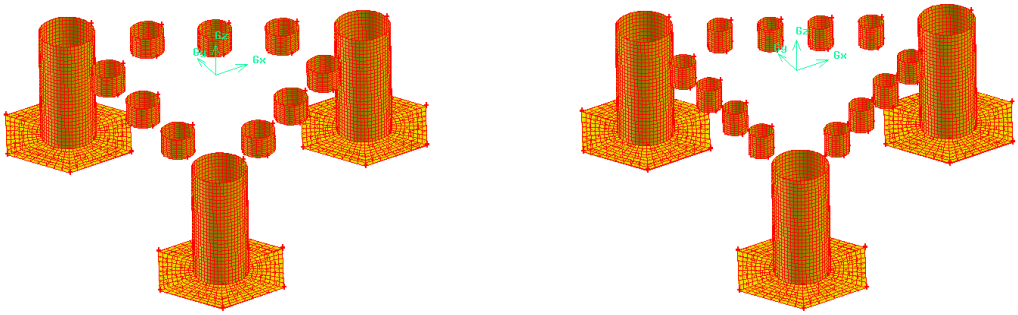

(a) 9 WECs (b) 12 WECs

Fig. 8 Mesh of the hybrid system for two different layouts of WECs.

The results presented in Section 4.2 are all for a single WEC. However, due to the presence of the platform and other WECs, the hydrodynamic coefficients, including the added mass, radiation damping and exciting force, may change. To illustrate the effects of the platform and other WECs, the ratio of the hydrodynamic coefficients for a single WEC to those for a hybrid system is introduced. Fig. 7 shows four examples of the layout of WECs on the same platform. Two meshes are shown in Fig. 8, where 128 elements are used on each WEC and 3313 elements on the platform, following a mesh convergence study. As the hybrid system and the incident wave are both symmetric about the x-plane, only some of the hydrodynamic coefficients for some typical WECs are presented. Four cases are chosen here to analyze the variation of hydrodynamic coefficients. The detailed parameters can be found in Table 3.

Table 3 Parameters of different layouts of WECs

Number of WECs	r [m]	d [m]	L_1 [m]	L_2 [m]
6	5.18	3.45	17.20	19.60
9	3.22	4.29	10.68	12.18
12	2.35	4.71	7.81	8.67
15	1.96	4.91	6.52	8.65

Fig. 9 - Fig. 11 show the variation of the ratios of added mass, radiation damping and wave

exciting force for the hybrid system to those for a single WEC. The added mass and radiation damping represent impedance to the motion of WECs. The difference observed in Fig. 9 - Fig. 11 is closely related to the different positions of the WECs.

Fig. 9 shows that almost all the ratios of added mass are close to 1.0 for the 12 and 15 WEC cases, indicating that for a thinner WEC, the effect of platform and other WECs on the added mass is very small. However, as the number of WECs decreases, and the diameter to draft ratio $2r/d$ increases, the fluctuation in the ratio becomes larger. The largest amplification factor of added mass is near 1.1 at ω=1.15 rad/s for the layout of 9 WECs in in Fig. 9 (c) and the reduction factor is close to 0.8 near the resonance frequency ω=1.27 rad/s for the layout of 6 WECs in Fig. 9 (d). The effect of the platform and other WECs on the added mass is closely related to the size of WECs, with larger WECs having a greater impact on the variation of added mass.

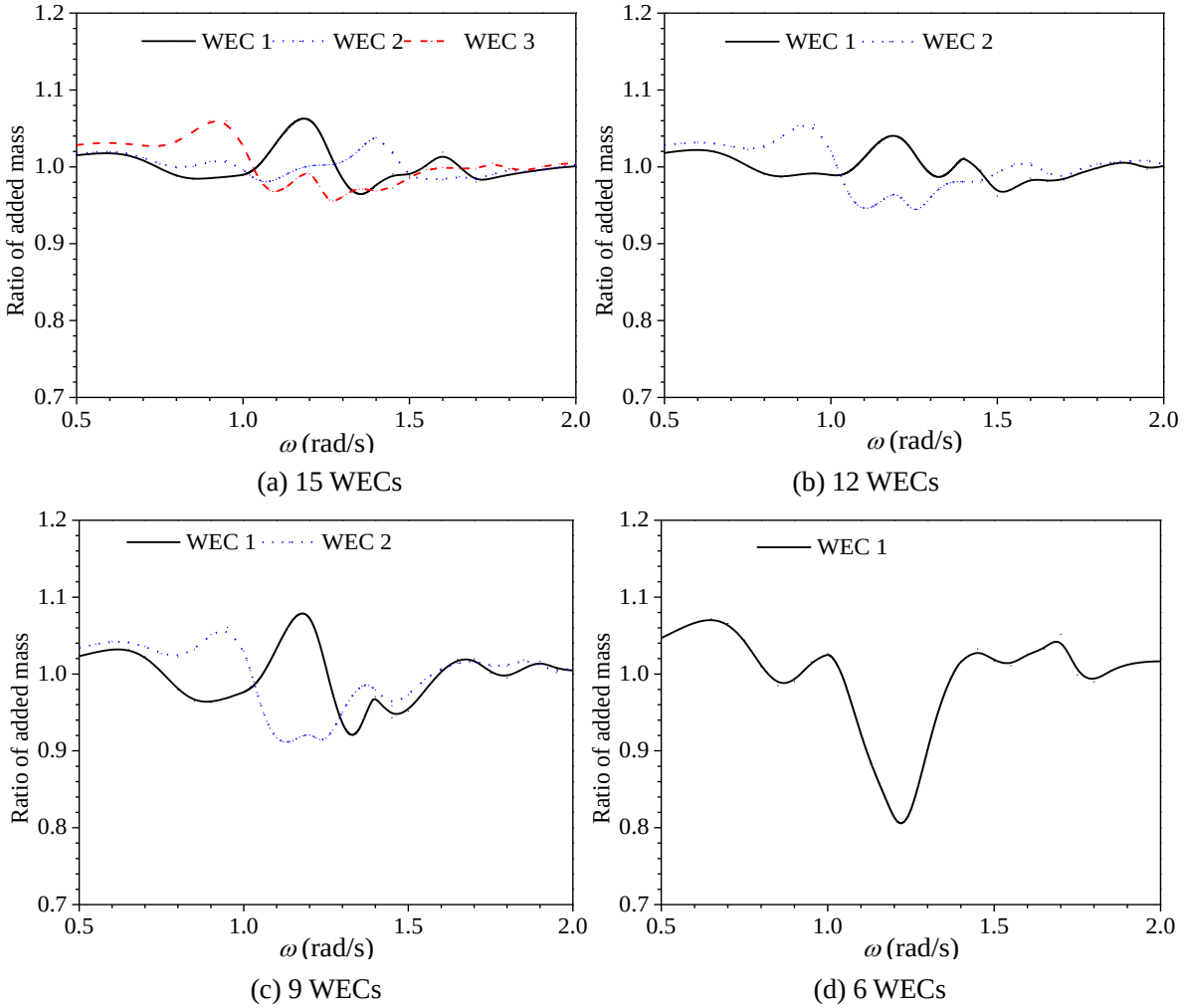

Fig. 9 Variation of the ratio of the added mass for the hybrid system to that for a single WEC.

Fig. 10 shows that the variation of radiation damping is smaller in the low frequency region than that in the high frequency region, because the sizes of the platform and WECs are

relatively smaller than the wave length in the low frequency region. The largest amplification factor of radiation damping is over 2.0 at ω=1.75 rad/s and the reduction factor is smaller than 0.5 near ω=1.3 rad/s both for the layout of 6 WECs. Thus, the effect of the platform and other WECs on the radiation damping is more significant than the added mass.

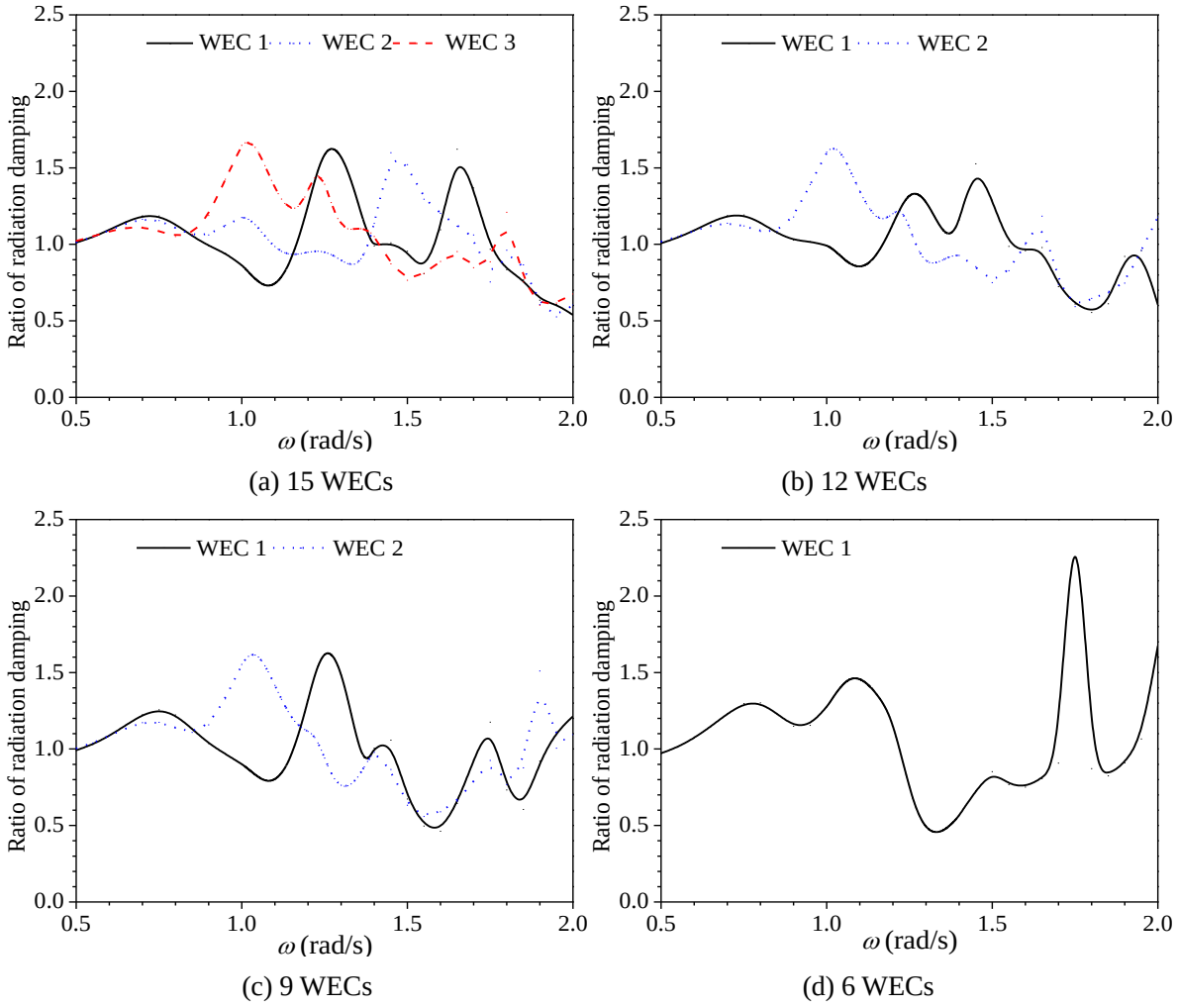

Fig. 10 Variation of the ratio of the radiation damping for the hybrid system to that for a single WEC.

Fig. 11 shows that the effect of the platform and other WECs on the wave exciting force is smaller in the low frequency region than that in the high frequency region, similar with the radiation damping. In addition, at most frequencies, the wave exciting forces acting on WECs in front of the platform are generally larger than those at the back due to the sheltering effect of the platform and other WECs. The largest wave exciting force amplification factor is larger than 2.0 for WEC 1 in front of the platform near ω=1.7 rad/s for nine WECs, which will directly influence the motion of the WEC. The largest reduction factor is below 0.2 for WEC 4 at the back of the platform near ω=1.6 rad/s for the nine WEC configuration. Consequently, the effect of the platform and other WECs on the wave exciting force can be significant, especially at higher frequencies, as their sizes are comparable to the wave length.

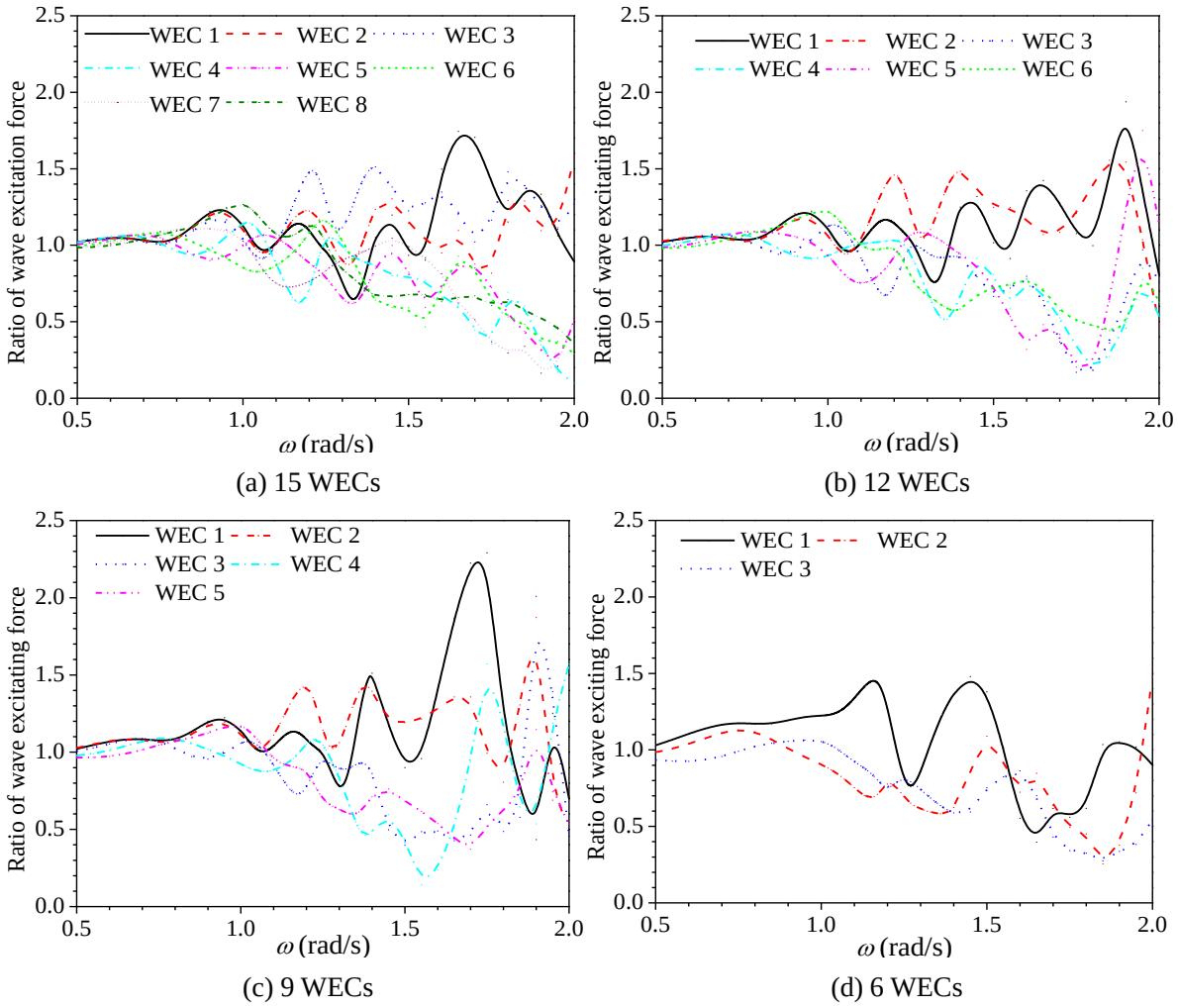

Fig. 11 Variation of the ratio of the wave exciting force for the hybrid system to that for a single WEC versus ω.

4.4 Variation of optimal PTO damping

To simplify the calculation procedure, many researchers have used the optimal PTO damping calculated by Eq. (8), where the added mass and radiation damping were obtained for a single WEC [23]. However, as shown in Fig. 9 and Fig. 10, the added mass and radiation damping can be significantly altered by the diffraction of the platform and other WECs. Therefore, the optimal PTO damping is different for each WEC. Meanwhile, Eq. (8) is only suitable for a single WEC. It is difficult to obtain an expression for the optimal PTO damping for each WEC due to the coupled motion equation of Eq. (2). Thus numerical evaluation is the preferred method to obtain the optimal PTO damping. If a different optimal PTO damping is considered for each WEC and M different PTO damping values are chosen for the optimization for each WEC, M^N evaluations will be required, which is time consuming. Therefore, to simplify the evaluation procedure, the same PTO damping for each WEC is assumed for the optimization in the present study, similar with the diagonal optimization in

[23]. Fig. 12 shows the ratio of optimal PTO damping for the hybrid system by numerical search method to that for the single WEC calculated based on Eq. (8), and the latter one is also given for the illustration. The optimal PTO damping is smallest near the resonance frequency (ω=1.27 rad/s). The difference between the optimal PTO damping determined through the numerical search method and Eq. (8) is significant near the resonance frequency, which will limit the total wave power of the hybrid system.

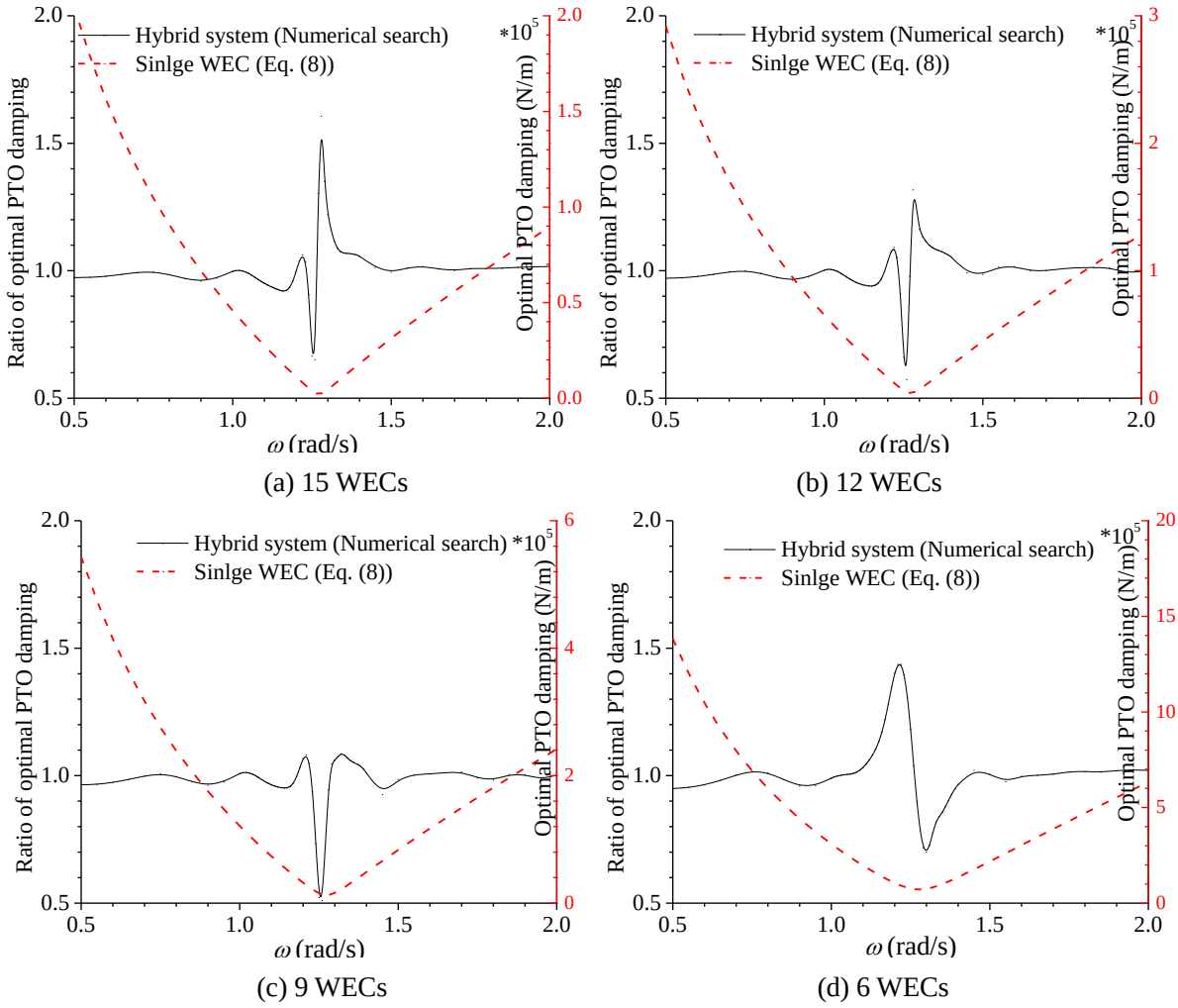

Fig. 12 Comparison of optimal PTO damping calculated by a single WEC and the hybrid system.

4.5 Viscous effect of WECs

As Section 3.2 introduced, the viscous radiation damping $\lambda_{\mathrm{vis},i}$ can be obtained through the free decay motion of the WEC, calculated by the Star-CCM software in the present paper. The detailed settings of the Star-CCM software can be found in [41][42]. The existence of the platform and other WECs may influence the radiation damping, similar with the potential flow theory analysis in Fig. 10. Accurate prediction of $\lambda_{\mathrm{vis},i}$, and the free decay motion of the WEC should be performed considering the existence of platform and other WECs, however

the computational time is excessive due to the large number of high-resolution meshes required. As a compromise, the viscous corrections calculated for a single WEC and the hybrid system are compared.

Taking $2r/d$=1.5 (9 WECs) as an example, the free decay motion of a single WEC is compared with the hybrid system, where only WEC 1 undergoes free decay motion while the platform and other WECs are fixed, as shown in Fig. 13. The radiation damping of WEC 1 calculated by WAFDUT and the Star-CCM+ is given in Table 4. Fig. 14 compares the total wave power at different wave frequencies between the potential flow results, the potential flow results with viscous correction for a single WEC and the potential flow results with viscous correction for the hybrid system. The uncorrected potential flow results significantly overestimate the total wave power, especially near the resonance frequency. The maximum total wave power based on uncorrected potential flow theory is close to 2.5 times of that of the potential flow theory with viscous correction for the hybrid system, whereas the results with viscous correction for a single WEC only overestimate the hybrid system by about 10%. To reduce the computation time, the viscous correction for a single WEC is adopted in the initial design. In the following sections, different $2r/d$ are chosen: [3.2, 3.0, 2.6, 2.4, 2.0, 1.5, 1.0, 0.8]. The corresponding $f_{\lambda,\mathrm{vist}}$ in Eq. (6) are shown in Fig. 15, calculated based on the method in Section 3.2. It can be seen that $f_{\lambda,\mathrm{vist}}$ generally decreases as $2r/d$ increases, implying that the viscous effect becomes smaller as the WEC becomes larger, similar with Chen et al.[32].

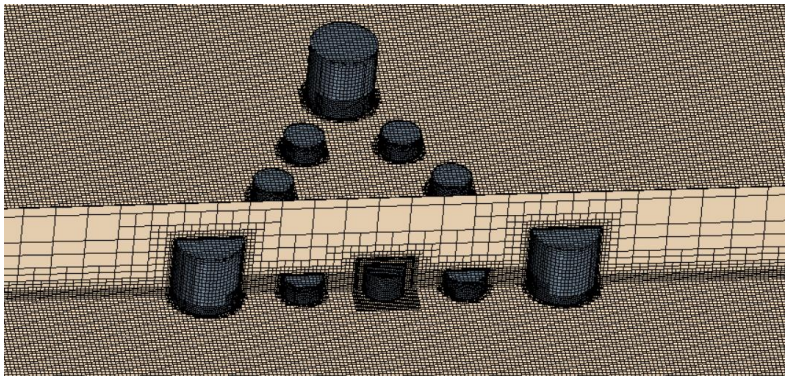

Fig. 13 Computation domain of the hybrid system for the free decay test.

Table 4 Computed radiation damping with and without viscous effects.

Type	λ_{ii} (kg/s)	λ_{vist}(kg/s)	$f_{\lambda,\mathrm{vist}}$
Single (WEC 1)	12339.90	38462.38	3.12
Hybrid system	20011.00	50021.71	2.50

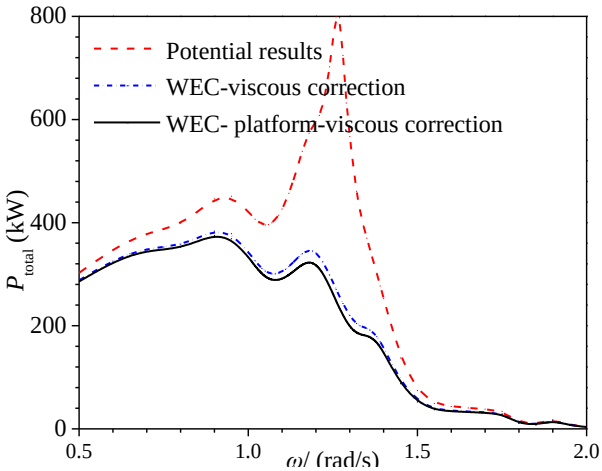

Fig. 14 Comparison of the total wave power vs. ω between the uncorrected potential flow results, the potential results with viscous correction for a single WEC and the potential results with viscous correction for the hybrid system.

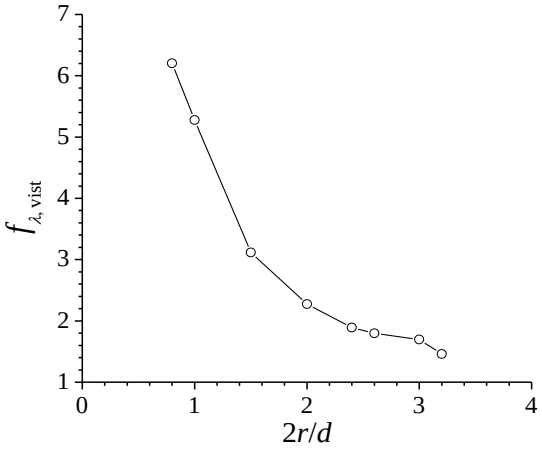

Fig. 15 Variation of non-dimensional viscous damping correction coefficient $f_{\lambda,\text{vist}}$ versus $2r/d$.

4.6 Wave power with different 2r/d

Fig. 16 compares the total wave power P_{total} at different wave frequencies with different WEC layouts based on potential flow theory and potential flow theory with viscous correction. The peak total wave power P_{total} decreases significantly for the thinner WECs near the resonance frequency, whereas the decrease is more slightly for the fatter WECs after considering the viscous correction. This is because the viscous damping correction becomes smaller as the WEC becomes fatter, as shown in Fig. 15. The potential flow results overestimate the wave power significantly near the resonance frequency. The maximum magnification factor is 3.97 for the thinnest WECs, compared to 1.09 for the fattest WECs. Fig. 16 (b) demonstrates that the total wave power P_{total} increases across almost all wave frequencies with the increase of $2r/d$. Moreover, the total wave power is generally large for

wave frequencies smaller than the resonance frequency (ω<1.27 rad/s), decreasing sharply in the high frequency region (ω>1.27 rad/s) for all 2r/d. Thus, in a limited region, the system with larger WECs will capture more wave energy despite the smaller number of WECs.

The wave power per unit weight P_{av} in Eq. (11) is introduced as a criterion of economic efficiency. The larger P_{av} means the higher economic efficiency. The wave power per unit weight P_{av} is given in Fig. 17 for the potential flow results without and with viscous correction. P_{av} calculated based on uncorrected potential flow theory follows a similar trend to the total wave power P_{total} (Fig. 16 (a)). When the viscous correction is applied, the peak P_{av} value is smaller at the resonance frequency and larger in the low frequency region as 2r/d increases. The difference among different 2r/d ratios is not large, indicating that there is little difference in the economic efficiency of the different device sizes.

The above results are obtained assuming the wave height is 2 m, and more results should be considered following the joint probability distribution of the wave height and period in Table 2. Fig. 18 shows the total wave power $P_{total(year)}$ and the wave power per unit weight $P_{av(year)}$ averaged over one year based on potential flow theory with viscous correction. The total wave power $P_{total(year)}$ increases significantly as 2r/d increases, while the wave power per unit weight $P_{av(year)}$ is almost unchanged. Thus, different layouts of WECs lead to very small differences in terms of economic efficiency, while the fatter WEC has the larger total wave power $P_{total(year)}$ in this sea state. To capture more wave energy it is therefore preferable to deploy fewer, larger WECs.

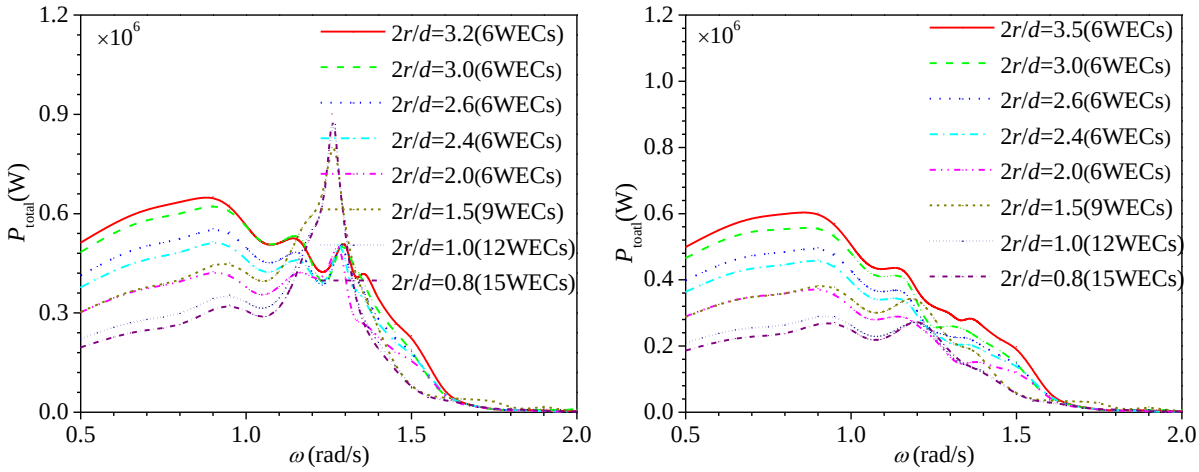

(a) Potential flow theory results (b) Potential flow theory results with viscous correction

Fig. 16 Variations of total wave power P_{total} versus ω with different 2r/d.

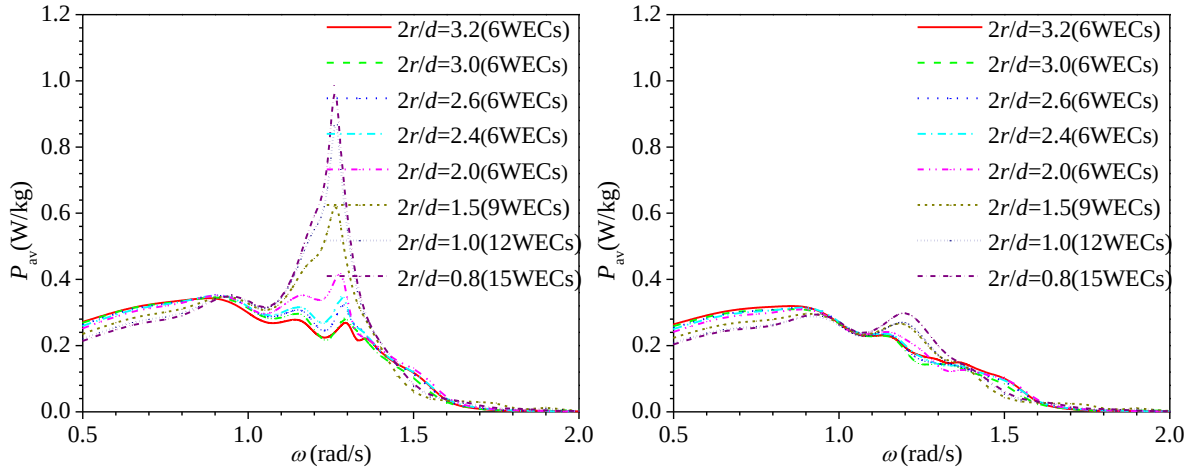

(a) Potential flow theory results (b) Potential flow theory results with viscous correction

Fig. 17 Variations of total wave power per unit weight P_{av} versus ω with different $2r/d$.

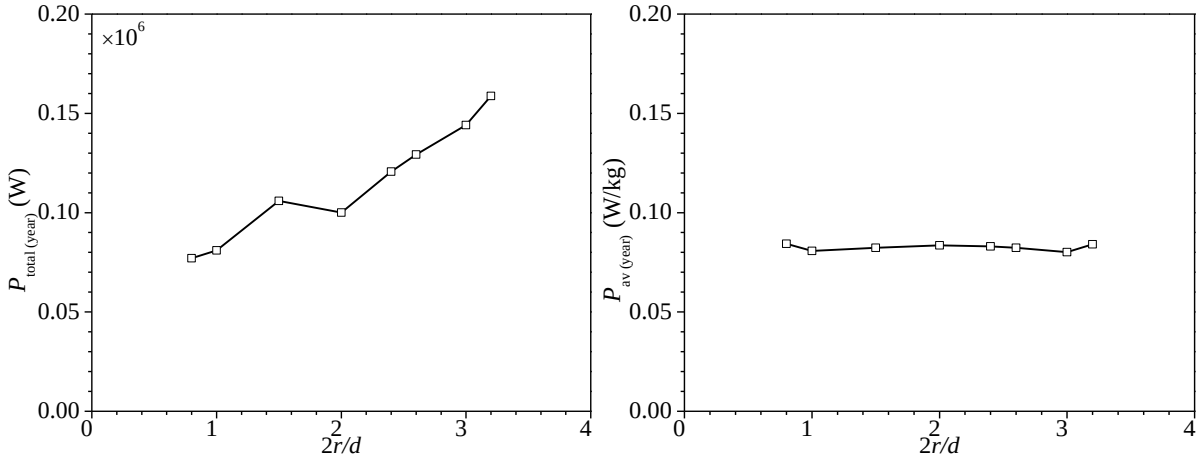

(a) Wave power (b) Wave power per unit weight

Fig. 18 Variations of annual total wave power $P_{total(year)}$ and annual wave power per unit weight $P_{av(year)}$ versus $2r/d$ based on potential flow theory with viscous correction.

The mean interaction factor q_{mean}, calculated by Eq. (14), is shown in Fig. 19 to investigate the effect of wave interactions on power absorption in a WEC array. The trends in Fig. 19 (a) and (b) are similar, except near the resonance frequency due to viscous effects. q_{mean} is close to 1.0 in the lower frequency region (ω<0.9 rad/s), which means the influence of the platform and other WECs is very small, as they are relatively smaller than the wave length at these frequencies. For ω=0.9 rad/s, the corresponding wave length is 76 m in infinite depth, which is much larger than the column diameter of 10.7 m and the largest WEC diameter of 10.78 m for $2r/d$=3.2. Moreover, the mean interaction factor q_{mean} changes more significantly for all $2r/d$ as the wave frequency increases. This is because when the size of the platform or WECs increases relative to the wave length, the effect of the platform and other WECs is amplified. q_{mean} is larger than 1.0 at some wave frequencies, but is generally smaller than 1.0, which

means the park effect is usually negative for the total power of the wave farm.

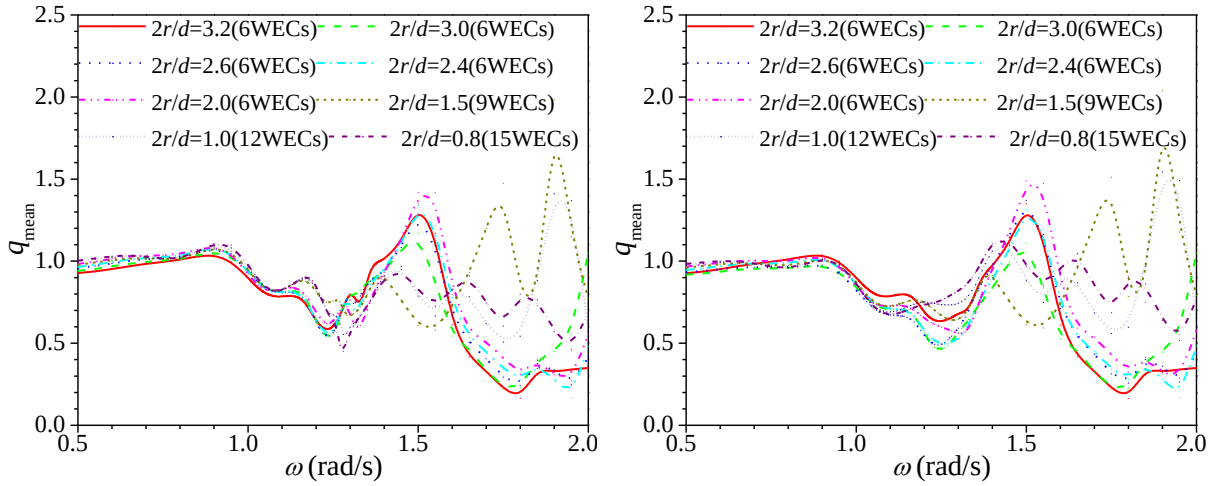

(a) Potential flow theory results (b) Potential flow theory results with viscous correction

Fig. 19 Variations of mean interaction factor q_{mean} versus ω with different $2r/d$.

4.7 Wave forces on the platform with different 2r/d

For a single fixed platform, only the exciting wave force acts on the platform. However, when WECs are installed on the fixed platform, the WECs change the exciting force acting on the platform, and the heave motion of the WECs exerts a radiation force on the platform. Additionally, constraining the motion of the WECs and platform in the horizontal direction leads to transmission of horizontal forces from the WECs to the platform. Unlike the horizontal force, only the vertical force from the WEC PTO system will react against the platform, since the WECs can move in heave motion. The pitch moment comes from the combined action of the horizontal and vertical forces.

Fig. 20 compares the horizontal, vertical forces and pitch moment for different WEC layouts, and the results of a single fixed platform are also given for reference. The design of platform is largely controlled by the maximum value of forces. The added horizontal force on WECs may increase the total horizontal forces acting on the platform, but because the WECs capture some of the wave energy of the flow field, the incident force may be reduced. Therefore, different trends may be observed for different wave frequencies. In general, the effect of adding WECs is to increase the horizontal force at most frequencies, while the maximum horizontal force near ω=1.05 rad/s decreases and becomes smaller as $2r/d$ increases, as shown in Fig. 20 (a).

Fig. 20 (b) shows that the maximum vertical force on the platform appears at the lowest frequency after adding WECs. As $2r/d$ increases, the vertical force on the platform increases more significantly in the region of ω<0.9 rad/s and ω>1.3 rad/s. For the hybrid system of WECs and platform, the vertical force is the result of the exciting force, the radiation force

due to WEC motion, and the PTO system.

Fig. 21 compares the single fixed platform, the fixed platform and WECs considering only the diffraction of the added WECs, the exciting force plus the radiation force due to motions of WECs, and the total vertical force including the PTO force. The vertical PTO force is the most important factor on the total vertical force on the platform. The PTO force is close related to the PTO damping and the velocity of WECs. The large PTO damping in the low wave frequency region shown in Fig. 12 results in a significant increase of vertical force on the platform, which is the main reason that the total vertical force on the platform increases so greatly.

Fig. 20 (c) shows that there are two peak values of pitch moment near ω=0.65 rad/s and ω=1.05 rad/s. After adding WECs, the pitch moment generally decreases at all wave frequencies, especially near ω<0.9 rad/s. The maximum pitch moment on the platform reduces compared with a single fixed platform near ω=1.05 rad/s, similar to the horizontal force. In the region of ω<0.9 rad/s, the horizontal and vertical forces both increase with increasing $2r/d$, and the vertical force increases much faster than the horizontal force. The pitch moment comes from the combined action of the horizontal force and the vertical force, but their effect on the pitch moment is in opposite directions. The pitch moment mainly comes from the contribution of horizontal force, and the rapid growth of vertical force reduces the total pitch moment, therefore the pitch moment deceases more rapidly as $2r/d$ increases. In other wave frequency regions, the horizontal force is much larger than the vertical force, so the variation is similar to the horizontal force.

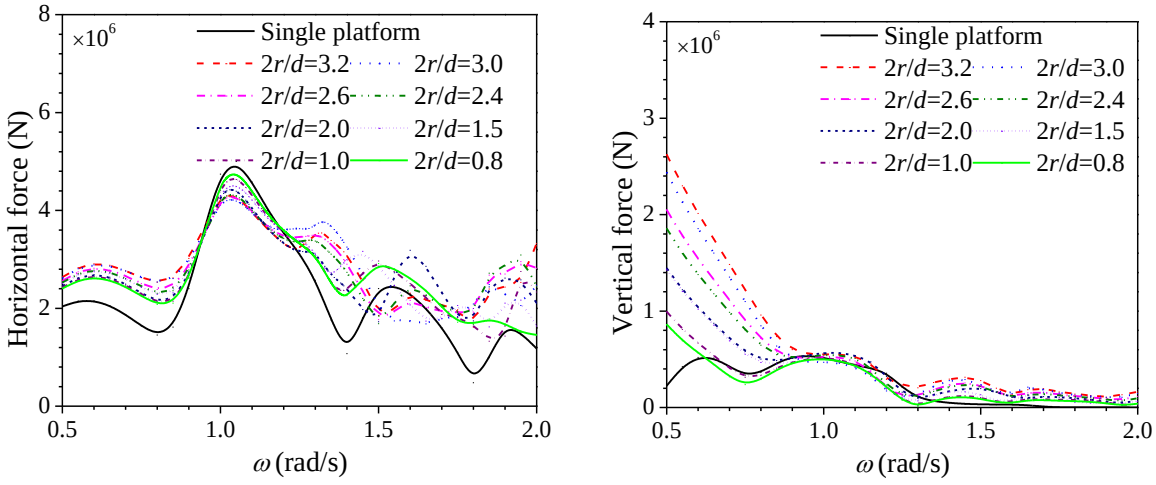

(a) Horizontal force

(b) Vertical force

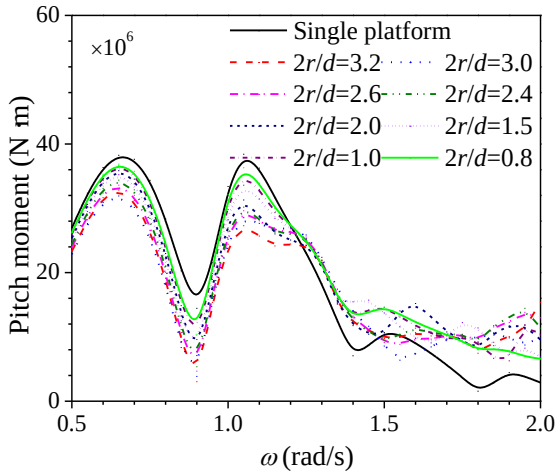

(c) Pitch moment

Fig. 20 Variations of horizontal force, vertical force, and pitch moment versus ω with different $2r/d$.

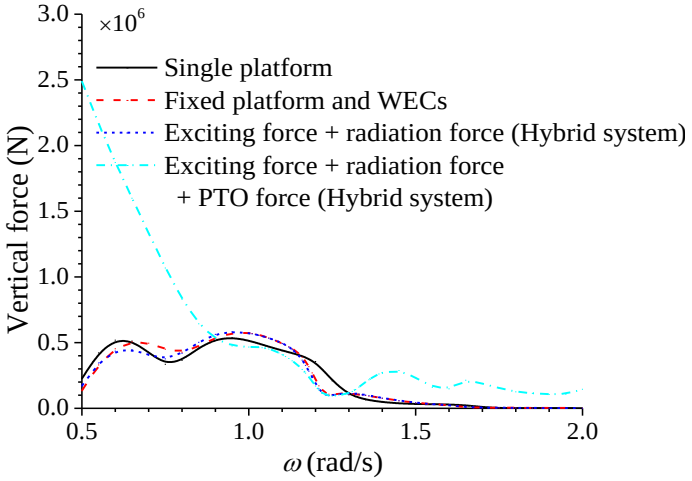

Fig. 21 Different components of vertical force for $2r/d$=3.2.

4.8 The effect of stiffness

It was observed in Fig. 16 (b) that the wave power is large when the wave frequency is smaller than the resonance frequency, and decreases sharply with increasing wave frequency. The joint probability distribution of wave height and period (Table 2), reaches up to 27.9% for the wave period T=4 s (ω=1.57 rad/s), while the corresponding wave power decreases below 7×10^4 W. Therefore, the WEC resonance frequency should be increased in order to capture more wave power in the wave environment as defined in Table 2. Eq. (7) shows that adding the PTO stiffness $k_{pto,\ i}$ increases the WEC resonance frequency. Taking $2r/d$=3.2 as an example, Fig. 22 compares the wave power with different PTO stiffnesses $k_{pto,i}$=0, 10^5 N/m, 2×10^5 N/m, and 5×10^5 N/m. Although the resonance frequency moves towards higher frequencies, the wave power decreases as the PTO stiffness $k_{pto,\ i}$ increases across most

frequencies, especially in the low frequency region. This is because the stiffness usually reduces the motion of the WECs. Therefore, the increased PTO stiffness reduces the wave power generally, and is not a desirable method to improve the average wave power.

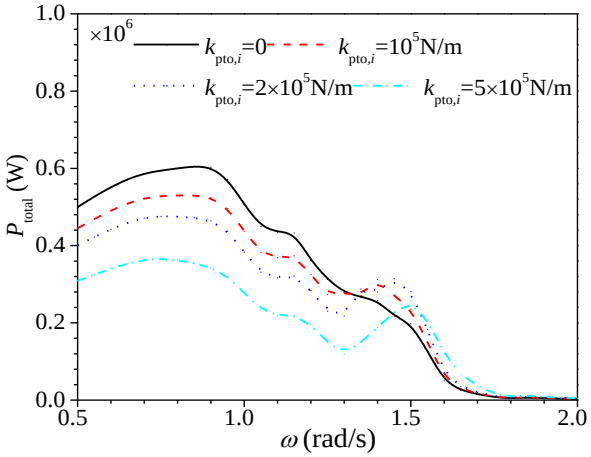

Fig. 22 Comparisons of wave power with different $k_{pto,\,i}$ for $2r/d$=3.2

4.9 Further optimization through changing WEC size

The PTO stiffness $k_{pto,\,i}$ generally reduces the wave power so $k_{pto,i}$ is chosen as 0 in this section. The other method to improve the wave power is to specify a larger value of ω_p in Eq. (19), and then the corresponding draft and radius can be obtained for a given $2r/d$. Fig. 18 shows that larger WECs absorb more wave power, therefore larger values of $2r/d$ are chosen for further study. Different typical wave periods T_p are specified to obtain the new WEC layout with the maximum radius constrained to be smaller than that of the column, as shown in Table 5. When T_p=3 s the maximum WEC radius is r=3.76 m, which is still much smaller than the radius of the column. This is because the radius and the draft both decrease if $2r/d$ continues to increase. The comparisons of total wave power P_{total} and total wave power per unit weight P_{av} at different wave frequencies with different typical wave periods are presented in Fig. 23. As the typical wave period T_p decreases, P_{total} decreases in the low frequency region and increases in the high frequency region except for T_p=4.0 s, while P_{av} increases significantly across the whole frequency range. The total annual wave power $P_{total(year)}$ and the wave power per unit weight $P_{av(year)}$ are obtained based on Table 2 and Eqs. (12) and (13), as shown in Table 5. For T_p=4.94 s, 4.50 s, 4.00 s, and 3.50 s, $P_{total(year)}$ is very similar, while $P_{av(year)}$ increases significantly as T_p decreases. However, $P_{total(year)}$ decreases significantly as the typical wave period continues to decrease to T_p=3.0 s although $P_{av(year)}$ remains increase throughout. Therefore, If the maximum wave power is the target, T_p=4.0 s is the best choice. If the wave power and the economic efficiency are both considered, T_p=3.5 s is the best.

Table 5 Parameters of different layouts of WECs

T_P (s)	ω_p (rad/s)	$2r/d$	N	r (m)	d (m)	L_1 (m)	L_2 (m)	$P_{total(year)}$(kW)	$P_{av\ (year)}$ (W/kg)
4.94	1.27	3.2	6	5.39	3.37	21.57	17.42	1.59×10^5	0.084
4.50	1.40	4.4	6	5.39	2.45	21.54	17.43	1.60×10^5	0.116
4.00	1.57	7.1	6	5.38	1.52	21.53	17.44	1.90×10^5	0.224
3.50	1.80	12.0	6	5.00	0.83	20.00	18.20	1.78×10^5	0.443
3.00	2.09	13.0	6	3.76	0.58	15.03	20.69	1.23×10^5	0.771

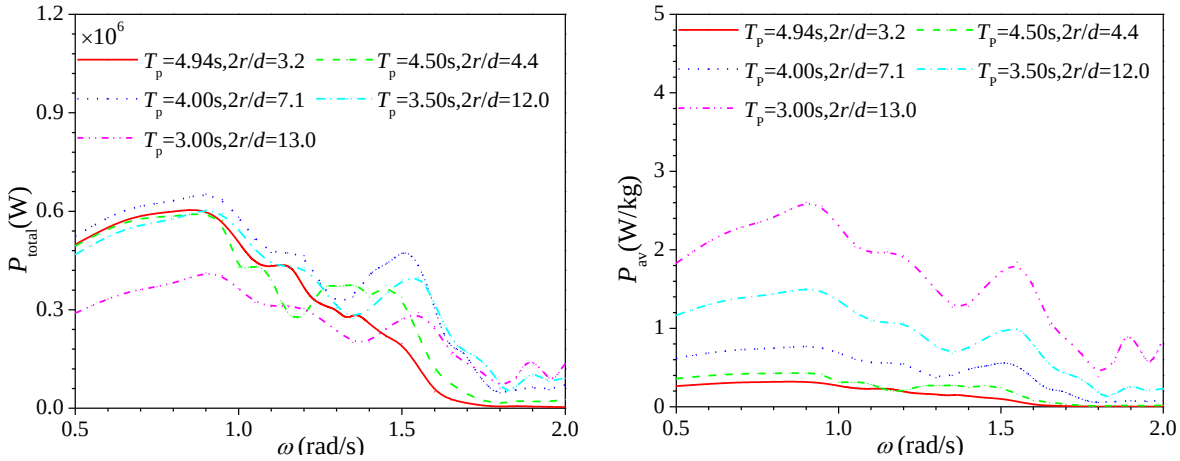

(a) Wave power (b) Wave power per unit weight

Fig. 23 Variations of total wave power P_{total} and total wave power per unit weight P_{av} versus ω with different typical wave periods T_P.

5. Conclusions

In this study, the potential flow theory with viscous correction in frequency domain is presented to investigate the hydrodynamic performance of a hybrid system combing a floating offshore wind platform and multiple heave-type WECs. The linear method is typically used for the initial design of floating offshore structures, because it can quickly and simply estimate the performance of the hybrid system. However, the further detailed design requires more accurate and sophisticated analysis, including nonlinear terms. The WindFloat platform and a target sea area around Shandong, China, are taken as examples for the optimization of the WEC arrangement. The total power $P_{total}(\omega)$, wave power per unit weight $P_{av}(\omega)$, the mean interaction factor $q_{mean}(\omega)$, the total wave power $P_{total(year)}$, and the wave power per unit weight $P_{av(year)}$ in a given wave environment are investigated respectively. The following conclusions can be drawn from this study:

(1) The effect of the platform and other WECs on the radiation damping and wave exciting force is more significant than the added mass, especially at higher wave frequencies. Larger WECs result in a more significant effect on the variation of added mass.

(2) Potential flow theory overestimates the wave power of WECs, especially near the resonance frequency of WECs. The viscous effect becomes smaller as the diameter to draft ratio of the cylindrical WEC increases.

(3) Larger WECs are preferred because they capture more wave energy in a limited region and a specific sea state, and the wave power per unit weight is very close to smaller devices, despite the smaller number of WECs.

(4) The park effect is more significant in the high frequency region. It is usually negative for the wave power of the wave farm even though positive effects do arise at some wave frequencies.

(5) The WECs increase the total vertical force on the platform across almost all wave frequencies due to the PTO force reacting on the platform. As the diameter to draft ratio increases, the total vertical force increases more significantly. The horizontal force increases at most frequencies as a result of the WECs, although the maximum horizontal force is slightly decreased at the resonance condition.

(6) The pitch moment on the platform generally decreases with the addition of WECs, which is good for the floating wind platform because the pitch motion of the floating wind platform has unfavourable effect on wind generation. Therefore, the added WECs not only increases the total power of the hybrid system, but also reduces the pitch motion of the floating wind platform due to the smaller driving pitch moment.

(7) The stiffness can be used as a variable to change the resonance frequency of WEC to adapt to the target sea area; however, it reduces the wave power because it often impedes the motion of WECs.

(8) By adjusting the typical wave frequency of WECs, the optimal size and layout of WECs in the hybrid system can be obtained for a given wave environment.

The present optimization method can be used to obtain the optimum number and layout of WECs in the real applications. It is suitable to different sea states and platforms. If the wave environment or the wind platform is changed, the similar steps are used to find the optimum number and layout of WECs. The present results can provide valuable guidance for combining offshore power supply and platform protection performance to deliver a hybrid WEC-platform system that achieves cost sharing, helping to make wave energy economically competitive and commercial-scale wave power operations possible.

Acknowledgement

This work was supported by the Natural Science Foundation of China (NSFC) through grant 51761135013, INNO-MPP project, the UK Engineering and Physical Sciences Research Council UK (EPSRC) and the Natural Environment Research Council UK (NERC), through

grant EP/R007497/1, the High-tech Ship Research Projects Sponsored by Ministry of Industry and Information Technology of the People's Republic of China-Floating Support Platform Project (the second stage) (MIIT201622), the Open Fund of Shandong Provincial Key Laboratory of Ocean Engineering, and the International Clean Energy Talent Program 2017 of China Scholarship Council.

References

[1] Wu XN, Hu Y, Li Y, Yang J, Duan L, Wang TG, et al. Foundations of offshore wind turbines: A review. Renew Sustain Energy Rev 2019; 104: 379-393.

[2] Mørk G, Barstow S, Kabuth A. Assessing the global wave energy potential. ASME 2010 29th International Conference on Ocean, Offshore and Arctic Engineering. American Society of Mechanical Engineers, 2010, 447-454.

[3] Liu YY, Yoshida S, Hu CH, Sueyoshi M, Sun L, Gao JL, et al. A reliable open-source package for performance evaluation of floating renewable energy systems in coastal and offshore regions. Energy conversion and Management, 2018, 174: 516-536.

[4] Pérez-Collazo C, Greaves D, Iglesias G. A review of combined wave and offshore wind energy. Renew Sustain Energy Rev 2015; 42(42):141-153.

[5] Astariz S, Iglesias G. Selecting optimum locations for co-located wave and wind energy farms. Part II: A case study. Energy Convers Manag 2016; 122: 599–608..

[6] Cradden L, Kalogeri C, Barrios IM, Galanis G, Ingram D, Kallos G, Multi criteria site selection for offshore renewable energy platforms, Renew Energy 2016; 87: 791-806.

[7] Astariz S, Iglesias G. Enhancing wave energy competitiveness through collocated wind and wave energy farms, A Rev. Shad. Eff. Energies, 2015, 7344-7366.

[8] Wave Star A S. Wave Star energy web page. Wave Star A S; 2012.

[9] Power-technology.com. Green ocean energy wave trader web page. Net Resources International—NIR; 2010.

[10] Renewable Energy Focus. Gravitational wave energy absorber presented web page. Renewable Energy Focus: ElsevierLtd; 2010.

[11] Gao Z, Wan L, Michailides C, Moan T, Soulard T, Bourdier S, Babarit A, O'Sullivan K, Lynch K, Murphy J. D4.6 –Synthesis –Modelling and Testing: Methodology and Validation. EU FP7 MARINA Platform Project. NTNU. 2014.

[12] Wan L, Gao Z, Moan T, Lugni C. Experimental and numerical comparisons of a combined wind and wave energy converter concept under operational conditions. Renew Energy 2016; 93: 87–100.

[13] Michailides C, Gao Z, Moan T. Experimental study of the functionality of a semisubmersible wind turbine combined with flap-type wave energy converters. Renew Energy 2016; 93: 675-690.

[14]O'Sullivan K, Murphy J. Techno-economic optimization of an oscillating water column array wave energy converter. Proc. Of the 10th European wave and tidal energy conference, Aalborg, Denmark. 2013.

[15]Jonkman J, Butterfield S, Musial W, Scott G. Definition of a 5-MW Reference Wind Turbine for Offshore System Development, Technical Report/TP-500e38060, National Renewable Energy Laboratory, 2009.

[16]Aubault A, Alves M, Sarmento A, Roddier D, Peiffer A. Modeling of an Oscillating Water Column on the Floating Foundation WindFloat. 30nd International Conference on Ocean, Offshore and Arctic Engineering. Rotterdam, The Netherlands, June 19-24, 2011,

[17]Peiffer A, Roddier D, Aubault A. Design of a Point Absorber inside the WindFloat Structure. 30nd International Conference on Ocean, Offshore and Arctic Engineering, Rotterdam, The Netherlands, 19-24June, 2011.

[18]Antoine P, Dominique R. Design of an oscillating wave surge converter on the windfloat structure. 4th International Conference on Ocean Energy, Dublin, October 17, 2012.

[19]Pelagic Power A S. W2Power web page; 2010.

[20]Lee H, Poguluri SK, Bae YH. Performance analysis of multiple wave energy converters placed on a floating platform in the frequency domain. Energies 2018: 11, 406-.

[21]Kim KH, Lee K, Sohn JM, Park SW, Choi JS, Hong K. Conceptual design of 10MW class floating wave-offshore wind hybrid power generation system. In Proceedings of the Twenty-fifth International Offshore and Polar Engineering Conference, Kona, HI, USA, June 21–26, 2015,.

[22]Taghipour R, Moan T. Efficient frequency-domain analysis of dynamic response for the multi-body wave energy converter in multi-directional wave. Proceedings of the eighteenth International Offshore and Polar Engineering Conference, Vancouver, BC, Canada, July 6-11, 2008.

[23]De Backer G, Vantorre M, Beels C, De Rouck J, Frigaard P. Power absorption by closely spaced point absorbers in constrained conditions. IET Renew. Power Gener 2010; 4(6): 579-591.

[24]Sarmiento J, Iturrioz A, Ayllón V, Guanche R, Losada IJ. Experimental modelling of a multi-use floating platform for wave and wind energy harvesting. Ocean Eng 2019; 173: 761-773.

[25]Michele S, Renzi E, Perez-Collazo C, Greaves D, Iglesias G. Power extraction in regular and random waves from an OWC in hybrid wind-wave energy systems. Ocean Eng 2019; 191:106519.

[26]Perez-Collazo C, Greaves D, Iglesias G. A novel hybrid wind-wave energy converter for jacket frame substructures. Energies 2018, 11 (3): 637-.

[27]Jin S, Patton R. Geometry influences on hydrodynamic responses of a heaving point absorber wave energy converter, European Wave and Tidal Energy Conference, EWTEC, Southampton, UK. 2017.

[28]Tom NM. Design and control of a floating wave-energy converter utilizing a permanent magnet linear generator, Ph.D. Thesis, University of California, Berkeley, 2013.

[29]Devolder B, Stratigaki V, Troch P, Rauwoens P. CFD simulations of floating point absorber wave energy converter arrays subjected to regular waves. Energies 2018; 11(3): 641-663.

[30]Son D, Belissen V, Yeung R W. Performance validation and optimization of a dual coaxial-cylinder ocean-wave energy extractor. Renew Energy 2016; 92: 192-201.

[31]Chen ZF, Zhou BZ, Zhang L, Li C, Zang J, Zheng XB, et al. Experimental and numerical study on a novel dual-resonance wave energy converter with a built-in power take-off system. Energy 2018; 165:1008-1020.

[32]Chen ZF, Zhou BZ , Zhang L , et al. Geometrical Evaluation on the Viscous Effect of Point-Absorber Wave-Energy Converters. China Ocean Eng 2018; 32(4): 443-452.

[33]Roddier D, Cermelli C, Aubault A,Weinstein A. WindFloat: A floating foundation for offshore wind turbines. J Renew Sustain Energy 2010; 2(3):53-.

[34]Zhou BZ, Wu GX, Meng QC. Interactions of fully nonlinear solitary wave with a freely floating vertical cylinder. Eng Anal Bound Elem 2016, 69: 119-131.

[35]Zhou BZ, Wu GX. Resonance of a tension leg platform excited by third harmonic force in nonlinear regular waves. Philos T Roy Soc A. 2015, 373: 20140105.

[36]Teng B, Taylor RE. New higher-order boundary element methods for wave diffraction/radiation. Appl Ocean Res 1995; 17: 71–77.

[37]Teng B, Gou Y, Wang G, Cao G. Motion response of hinged multiple floating bodies on local seabed. In Proceedings of the 24th International Society of Offshore and Polar Engineers (ISOPE), Busan, Korea, 2014.

[38]Sun SY, Sun SL, Wu GX. Fully nonlinear time domain analysis for Hydrodynamic performance of an oscillating wave surge converter. China Ocean Eng 2018; 32(5): 582-592.

[39]Budal K. Theory for absorption of wave power by a system of interacting bodies. J Ship Res 1977; 21:248–253.

[40]Bellew S. Investigation of the Response of Groups of Wave Energy Devices. Ph.D. Thesis, University of Manchester, Manchester, UK, 2011.

[41]Zhang HM, Zhou BZ, Vogel CR, Willden RHJ, Zang J, Zhang L. Hydrodynamic performance of a floating breakwater as an oscillating-buoy type wave energy converter. Appl Energy 2020; 257: 113996.

[42]Zhang HM, Zhou BZ, Vogel CR, Willden RHJ, Zang J, Geng J. Hydrodynamic performance of a dual-floater hybrid system combining a floating breakwater and an oscillating-buoy type wave energy converter. Appl Energy 2020; 259:114212.